NANO LETTERS

Letter

pubs.acs.org/NanoLett

$(Ga_{1-x}Zn_x)(N_{1-x}O_x)$ Nanocrystals: Visible Absorbers with Tunable Composition and Absorption Spectra

Kyureon Lee, Bryan M. Tienes, Molly B. Wilker, Kyle J. Schnitzenbaumer, and Gordana Dukovic*

Department of Chemistry and Biochemistry, University of Colorado Boulder, Boulder, Colorado 80309, United States

Supporting Information

ABSTRACT: Bulk oxy(nitride) $(Ga_{1-x}Zn_x)(N_{1-x}O_x)$ is a promising photocatalyst for water splitting under visible illumination. To realize its solar harvesting potential, it is desirable to minimize its band gap through synthetic control of the value of x. Furthermore, improved photochemical quantum yields may be achievable with nanocrystalline forms of this material. We report the synthesis, structural, and optical characterization of nanocrystals of $(Ga_{1-x}Zn_x)(N_{1-x}O_x)$ with the values of x tunable from 0.30 to 0.87. Band gaps decreased from 2.7 to 2.2 eV over this composition range, which corresponded to a 260% increase in the fraction of solar photons that could be absorbed by the material. We achieved nanoscale morphology and compositional control by employing mixtures of $ZnGa_2O_4$ and ZnO nanocrystals as synthetic precursors that could be converted to $(Ga_{1-x}Zn_x)(N_{1-x}O_x)$ under NH_3. The high quality of the resulting nanocrystals is encouraging for achieving photochemical water-splitting rates that are competitive with internal carrier recombination pathways.

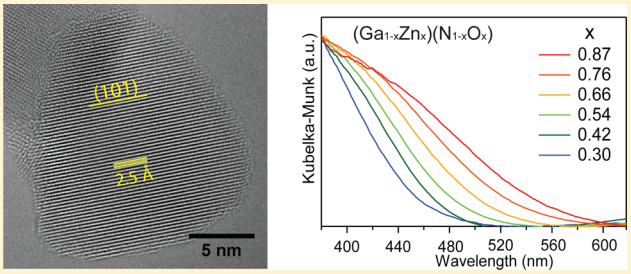

KEYWORDS: *Photocatalysis, water splitting, oxy(nitrides), nanocrystals*

In the bulk form, the oxy(nitride) $(Ga_{1-x}Zn_x)(N_{1-x}O_x)$ has recently emerged as a promising photocatalyst for water splitting at wavelengths >400 nm.[1−4] This material is a solid solution of ZnO and GaN and has the rare combination of visible absorption, appropriate band edges for the reduction and oxidation half-reactions required for water splitting, and resistance to photocorrosion.[1−4] For the purposes of solar energy harvesting, it is necessary to decrease its band gap while maintaining sufficient driving force for water splitting. It is not well understood why $(Ga_{1-x}Zn_x)(N_{1-x}O_x)$ exhibits visible absorption given that GaN and ZnO have band gaps of 3.4 and 3.3 eV, respectively.[5−17] There is even disagreement between experimental reports of how bulk $(Ga_{1-x}Zn_x)(N_{1-x}O_x)$ band gaps depend on composition.[5,18] In materials prepared by mixing ZnO and GaN powders under high pressures and temperatures, the oxy(nitride) with $x = 0.49$ had a lower band gap (~2.5 eV) than both GaN-rich ($x = 0.22$) and ZnO-rich ($x = 0.76$) materials.[5] This behavior is known as band gap bowing. In contrast, in $(Ga_{1-x}Zn_x)(N_{1-x}O_x)$ synthesized by nitridation of layered double Zn^{2+} and Ga^{3+} hydroxides, the band gap decreased over the $0.46 < x < 0.81$ range, to as low as 2.37 eV.[18] This difference in behavior is not understood, and it has important implications for how much of the solar spectrum can be harvested by the oxy(nitrides).

In addition to control of composition and absorption spectra, it is desirable to reduce the sizes of oxy(nitride) particles from the submicrometer bulk regime to dimensions around 10 nm. In bulk $(Ga_{1-x}Zn_x)(N_{1-x}O_x)$ functionalized with a H^+ reduction cocatalyst, the water-splitting quantum yield is governed by the competition between carrier migration, surface redox reactions, and carrier trapping and recombination.[3,19] The highest reported quantum yield of water splitting under visible illumination is 6%.[20] Nanocrystalline oxy(nitrides), with dimensions comparable or smaller than the mean free paths of electrons and holes in the material, may exhibit improved photochemical quantum yields. Because of high surface area-to-volume ratios and the lack of grain boundaries, the probability that a carrier would reach a catalytic surface site rather than decay via energy wasting relaxation pathways may be higher in nanocrystals than in the bulk form. Similar advantages of nanostructures over the bulk material have been demonstrated for Fe_2O_3 and $KCa_2Nb_3O_{10}$.[21,22] However, synthetic methods for oxy(nitrides) with sub-100 nm dimensions are scarce.[23−25] Notably, Han et al. have reported synthesis of nanoparticles with diameters as low as 10 nm and values of x up to 0.48.[23] Oxy(nitride) nanocrystals with a wide range of compositions have not been previously reported. In particular, because of the possibility of achieving lowest band gaps at high values of x,[18] ZnO-rich oxy(nitride) nanocrystals may be particularly suitable for solar water splitting.

In this letter, we describe a synthetic method that produces nanocrystals of $(Ga_{1-x}Zn_x)(N_{1-x}O_x)$ with an unprecedented range of compositions ($0.30 < x < 0.87$). Our strategy was to use nanocrystalline $ZnGa_2O_4$ and ZnO as precursors in varying ratios and convert them to the oxy(nitride) by exposure to NH_3. The required nitridation temperatures were lower than

Received: April 9, 2012
Revised: May 4, 2012
Published: May 23, 2012

   dx.doi.org/10.1021/nl301338z | *Nano Lett.* 2012, 12, 3268−3272

those needed for the synthesis of the bulk material, which allowed the nanoscale morphology to remain intact while producing high-quality crystals. The resulting materials were characterized by transmission electron microscopy (TEM), powder X-ray diffraction (XRD), diffuse reflectance spectroscopy, and samples with x = 0.76 were imaged by aberration-corrected high-resolution TEM. The dependence of lattice parameters on x was found to deviate from Vegard's law, in agreement with theoretical predictions.[12] The band gaps of these visible absorbers decreased continuously with increasing x, from 2.7 eV for x = 0.30 to 2.2 eV for x = 0.87. The fraction of solar photons that can be absorbed increases by 260% over this range, demonstrating the solar-energy harvesting potential of ZnO-rich oxy(nitride) nanocrystals. The contrast with previously reported band gap bowing in bulk oxy(nitrides) synthesized at high pressures[5] can be attributed to the formation of lower-density structures during nitridation reactions at atmospheric pressure.

Synthesis and characterization of nanocrystalline $ZnGa_2O_4$,[26] ZnO,[27] and $(Ga_{1-x}Zn_x)(N_{1-x}O_x)$ is described in detail in Supporting Information. $ZnGa_2O_4$ nanocrystals had the diameters of 3.6 ± 1.0 nm (Figure S1a, Supporting Information) and were soluble in organic solvents. The ZnO particles were larger (d = 10.6 ± 2.1 nm) (Figure S1c, Supporting Information) and were dispersible in ethanol. To ensure mixing of the two precursors, we adapted ligand-exchange procedures for CdS[28] to $ZnGa_2O_4$ and obtained water-soluble nanoparticles capped with 3-mercaptopropionic acid. Mixtures of these starting materials were treated with NH_3 in a quartz tube furnace for 10 h at temperatures above 500 °C to yield the oxy(nitride) product.

Role of Nitridation Temperature. The optimal temperature for the synthesis of nanoscale $(Ga_{1-x}Zn_x)(N_{1-x}O_x)$ depends on the interplay of several competing factors. At relatively low nitridation temperatures, the chemical transformation of $ZnGa_2O_4$ and ZnO nanocrystals to the oxy(nitride) is slow because of a combination of insufficient energy to overcome the nitridation activation barrier and the slow diffusion of atoms both within and between nanocrystals. At relatively high temperatures, nanoparticles can fuse into the bulk form. Additionally, evaporation of Zn^0 at high temperatures (~900 °C) has plagued the commonly used bulk oxy(nitride) synthesis and limited the available x to <0.4.[1−3,29] The optimal temperature balances these factors, ideally allowing complete precursor transformation into the oxy(nitride) without loss of Zn, while maintaining nanoscale morphology.

Powder XRD patterns of the nitridation product as a function of temperature are shown in Figure 1. Because longer reaction times can compensate for lower temperatures, all nitridations discussed here were carried out for 10 h. The starting material was a mixture of cubic spinel $ZnGa_2O_4$ and wurtzite ZnO with Zn content (Zn/(Zn + Ga)) of 0.38, as determined by elemental analysis of acid-digested samples using inductively coupled plasma optical emission spectroscopy (ICP-OES). At 500 °C, the product XRD pattern is very similar to that of the starting material. With increasing temperatures, increasing fractions of the wurtzite phases are observed, and cubic spinel phase is not detectable at temperatures ≥650 °C. This is most evident as the disappearance of the peak at 2Θ = 43°. The enlarged view of the region around 2Θ = 32° shows the appearance of the wurtzite (100) peak with increasing temperature. At 650 °C,

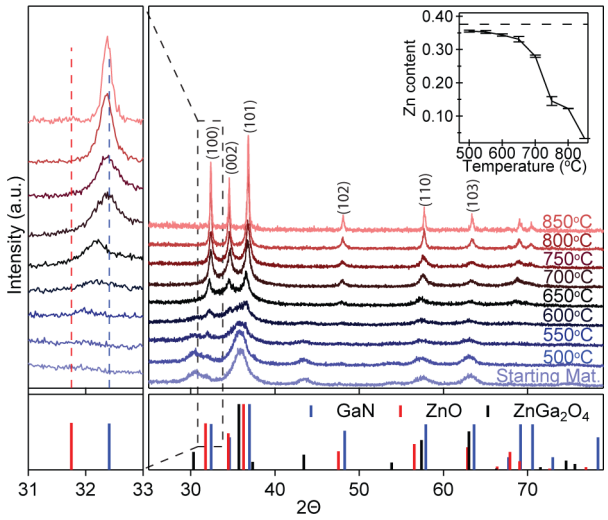

Figure 1. Powder XRD patterns of the products of nitridation of a mixture of $ZnGa_2O_4$ and ZnO nanocrystals at varying reaction temperatures. The Zn content (Zn/(Zn + Ga)) in the starting material was 0.38. Reference patterns for cubic spinel $ZnGa_2O_4$ (JCPDS #38-1240), wurtzite ZnO (JCPDS #05-0664), and wurtzite GaN (JCPDS #2-1078) are shown as vertical lines. Assignments for the wurtzite peaks are also shown. (Inset) Values of x as a function of nitridation temperature. The x in the starting material is shown by the dashed line.

there is a relatively broad peak centered between ZnO and GaN (100) positions, and it shifts toward GaN at higher temperatures. This peak also narrows with increasing temperature, indicating an increase in the crystallite size. The XRD data suggest that the conversion to $(Ga_{1-x}Zn_x)(N_{1-x}O_x)$ is complete at 650 °C, and higher temperatures lead to decreased Zn fraction. Elemental analysis of the nitridation products indeed shows a precipitous decline in Zn content at temperatures above 650 °C (Figure 1 inset) due to the Zn^0 evaporation described previously.[2,23,29] Temperatures required for synthesis of bulk oxy(nitrides) by nitridation are typically higher (>800 °C).[1−4,18] The chemical transformation of nanocrystalline precursors is faster likely due to higher surface energies and to the relatively short atomic diffusion distances necessary to obtain oxy(nitride) nanocrystals.

Control of Oxy(nitride) Composition. To obtain nanoscale $(Ga_{1-x}Zn_x)(N_{1-x}O_x)$ with a wide range of x, we combined nanocrystals of $ZnGa_2O_4$ and ZnO in varying ratios. The mixtures were then subject to nitridation at 650 °C for 10 h. Values of x in starting materials and products were determined by ICP-OES of acid-digested samples (Table S1, Supporting Information). No significant loss of Zn during nitridation was observed. TEM images of oxy(nitrides) with x = 0.54, 0.66, 0.76, and 0.87 and the corresponding size analysis are shown in Figure S2, Supporting Information. The particles appear faceted and reminiscent of hexagonal-cone shaped ZnO nanocrystals.[30] Particle sizes remained constant over the composition range, with dimensions around 18 nm and standard deviations ~5 nm. In this size regime, we do not expect to observe effects of quantum confinement because the exciton Bohr radii in ZnO and GaN are <5 nm.

XRD patterns of nanoscale $(Ga_{1-x}Zn_x)(N_{1-x}O_x)$ with x ranging from 0.30 to 0.87 are shown in Figure 2. The product with x = 0.30 exhibits poor crystallinity for reasons that we do not yet understand. It was also observed in bulk oxy(nitrides)

dx.doi.org/10.1021/nl301338z | Nano Lett. 2012, 12, 3268−3272

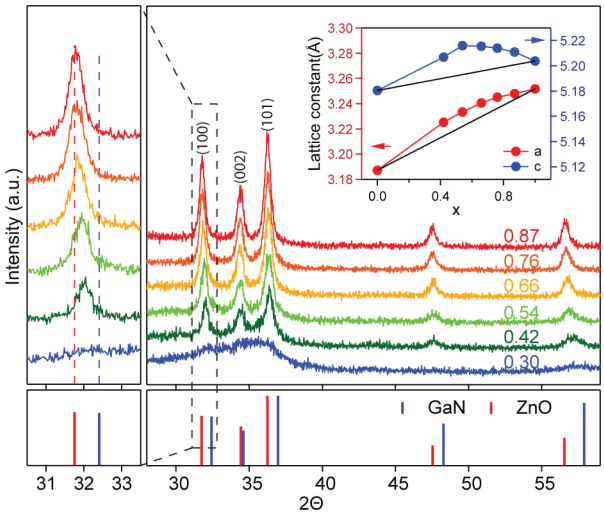

Figure 2. Powder XRD patterns of $(Ga_{1-x}Zn_x)(N_{1-x}O_x)$ with varying values of x, synthesized at 650 °C. Enlarged view of the wurtzite (100) peak shows a peak shift away from GaN and toward ZnO with increasing x. (Inset) Lattice parameters a and c, determined from positions of (100) and (002) peaks, respectively, showing deviations from ideal solid solution behavior represented by the black lines. Lattice parameters could not be determined for the x = 0.30 sample due to poor crystallinity.

that addition of ZnO to the starting material improved product crystallinity and photocatalytic activity, even though the remaining Zn fraction was <0.3, but the reason for this improvement is not known.[31] Oxy(nitrides) with x values of 0.42, 0.54, 0.66, 0.76, and 0.87 exhibit well-defined single wurtzite peaks in the XRD, indicating the presence of one product. An enlarged view of the (100) peak shows its position shifting away from GaN and toward ZnO with increasing x.

The variation of lattice constants a and c, determined from positions of (100) and (002) XRD peaks, respectively, is shown in the inset of Figure 2. Both lattice constants deviate from the linear ideal solid solution behavior described by Vegard's law. Similar deviations were predicted theoretically for bulk $(Ga_{1-x}Zn_x)(N_{1-x}O_x)$ and were attributed to bond distortions that arise because of the nonisovalent nature of the solid solution.[12] The deviations in Figure 2 are also similar, though somewhat higher in magnitude, to those seen in bulk $(Ga_{1-x}Zn_x)(N_{1-x}O_x)$ made by mixing of ZnO and GaN under high pressures (up to 6.2 GPa) and high temperatures (>700 °C).[5] One major difference is the lattice constant c for materials with approximately equal amounts of ZnO and GaN: in the bulk, the x = 0.49 was closer to the value for the ideal solid solution than the GaN- and ZnO-rich samples,[5] while in Figure 2 x = 0.54 is the furthest from the ideal value. This contrast implies that the chemical bonds in the c direction in x~0.5 samples are relatively long in our materials and relatively short in those obtained by high-pressure mixing of ZnO and GaN powders, suggesting structural differences and possibly even different phases of the material in the two experiments. The atomic level structure of $(Ga_{1-x}Zn_x)(N_{1-x}O_x)$, including the nature of the local chemical bonding, the spatial distribution of the constituent elements, and the balance between the enthalpic cost of mixed valence and the entropic benefit of mixing, is not yet understood.[5,6,10,12−14,32,33] Nevertheless, differences in the reaction pressures can account for the longer bonds observed here: high-pressure conditions generally favor higher-density phases, while the atmospheric pressure nitridation described here produces a more expanded lattice, especially in the x ~ 0.5 case. There may be additional differences in pressure response due to the nanoscale size regime,[34] but they are outside the scope of this letter.

Particle Crystallinity. To illustrate the crystalline quality of the materials described here, we focus on samples with x = 0.76. Aberration-corrected HRTEM images of three particles are shown in Figure 3. The particles are single crystalline, and their lattice spacings can be indexed to wurtzite, consistent with the XRD patterns (Figure 2). Crystallite size analysis by the Scherrer method[35] is consistent with the nanoparticle sizes measured from low-resolution TEM images (Figure S2c, Supporting Information), suggesting that most of these $(Ga_{1-x}Zn_x)(N_{1-x}O_x)$ nanoparticles are single crystalline. The high quality of the nanocrystals is promising for achieving improved water-splitting quantum yields because of the decreased probability of energy-wasting internal carrier trapping and recombination processes.

Optical Spectra as a Function of Composition. The ability to control x in $(Ga_{1-x}Zn_x)(N_{1-x}O_x)$ nanocrystals allowed us to also tune their absorption spectra, as shown in Figure 4. The spectra were obtained by conversion of diffuse reflectance to absorbance using the Kubelka−Munk function. A

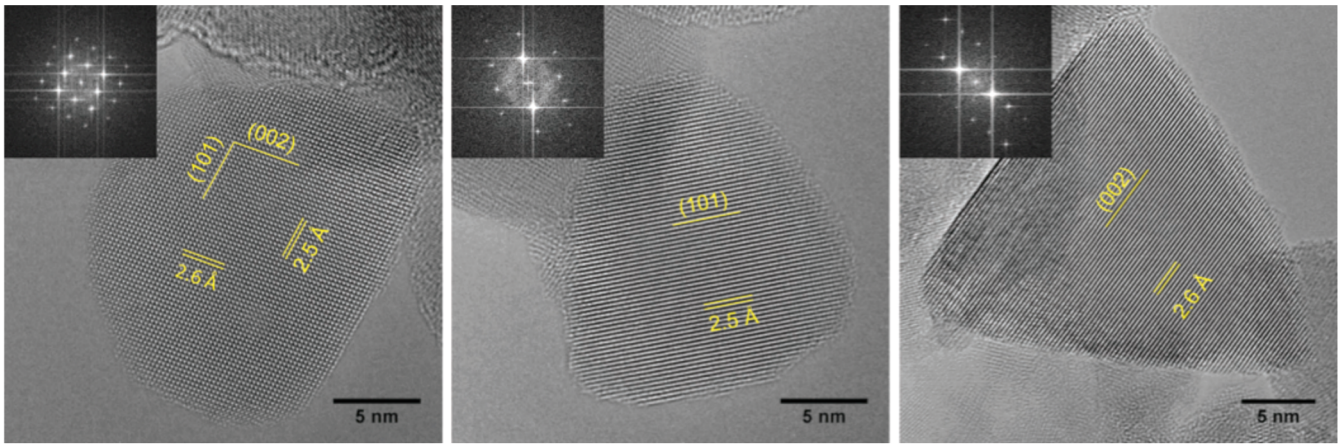

Figure 3. Aberration-corrected HRTEM images of $(Ga_{1-x}Zn_x)(N_{1-x}O_x)$ nanocrystals, with fast Fourier transforms of each particle (insets). Particles are single crystalline, and lattice spacings can be indexed to the wurtzite d-spacings consistent with XRD patterns.

dx.doi.org/10.1021/nl301338z | Nano Lett. 2012, 12, 3268−3272

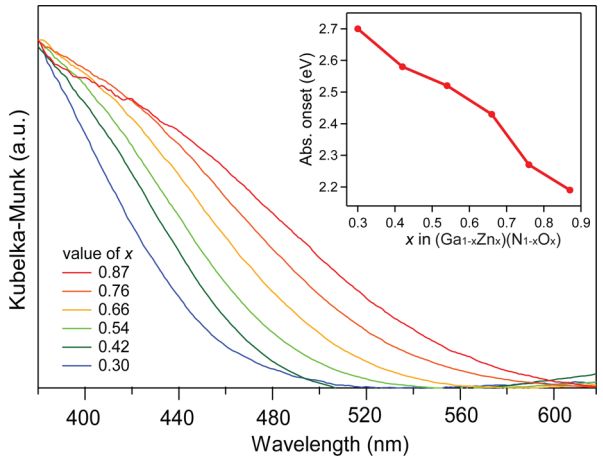

Figure 4. Absorption spectra of $(Ga_{1-x}Zn_x)(N_{1-x}O_x)$ with varying x, normalized at 380 nm. The absorption shifts continuously to longer wavelengths with increasing x. (Inset) Values of absorption onset as a function of x.

photograph of the samples (Figure S3, Supporting Information) shows the gradual change of color from yellow to orange with increasing x. The origin of the visible absorption in $(Ga_{1-x}Zn_x)(N_{1-x}O_x)$ is not well understood.[5−17] Furthermore, both band gap bowing and the improved band gap lowering in ZnO-rich oxy(nitrides) have been predicted by theoretical studies.[7,9,10,12] We made no assumptions about the direct or indirect nature of the visible absorption and simply reported the absorption onset values, determined by linear extrapolation of the absorption edge to zero absorbance (Figure 4 inset).[36] The absorption onset shifts to the red almost linearly from 460 nm (2.7 eV) for x = 0.30 to 565 nm (2.2 eV) for x = 0.87. This observation is in contrast to the case of bulk $(Ga_{1-x}Zn_x)(N_{1-x}O_x)$ synthesized by mixing of ZnO and GaN powders under high pressure and temperature, which exhibited band gap bowing with the minimum gap at x = 0.49 (2.5 eV).[5] Instead, our results agree with the observation for bulk $(Ga_{1-x}Zn_x)(N_{1-x}O_x)$ synthesized by nitridation of layered double hydroxides, which had red-shifting absorption onsets over the range $0.46 < x < 0.81$, to values as low as 2.37 eV.[18] We attribute this qualitatively different behavior to the structural differences between the high-pressure oxy(nitrides) and those obtained under atmospheric pressure, described above. The results reported here demonstrate that achieving ZnO-rich compositions of nanoscale oxy(nitrides) is an attractive strategy for band gap lowering. We do not yet know the value of x at which the band gap starts approaching that of pure ZnO.

The ability to synthesize oxy(nitride) nanocrystals with high ZnO content and lower band gaps has important practical implications. Because the solar photon flux rises sharply across the 300−550 nm range, relatively small differences in absorption onsets in this region can significantly impact the solar-harvesting capacity of a material. A semiconductor with a band gap of 2.7 eV can absorb 5.8% of terrestrial solar photons, while one with a band gap of 2.2 eV can absorb 15.3%.[37] Thus, a shift in the absorption onset between our x = 0.30 and 0.87 samples increases the fraction of solar photons that can be absorbed by a factor of 2.6. If the quantum yields of water splitting were otherwise equal (i.e., if the shifted band edges still had proper overpotentials for water splitting), this shift translates to 260% more H_2 that could be produced by the same amount of material under identical solar irradiation. One potential caveat is the effect of increased ZnO concentration in the solid solution on particle stability. ZnO is known to be susceptible to anodic photocorrosion.[38] Because of the limited range of compositions available, literature examples of the use of $(Ga_{1-x}Zn_x)(N_{1-x}O_x)$ for photocatalytic water splitting focus on GaN-rich materials.[1,2] In these cases, the photocatalysts were stable for more than 15 h during water splitting in acidic media.[1,2,39] Mixing GaN and ZnO into a solid solution provides resistance to photocorrosion and it remains to be seen whether this phenomenon extends to ZnO-rich oxy(nitrides).

In summary, we have reported the synthesis and characterization of high-quality $(Ga_{1-x}Zn_x)(N_{1-x}O_x)$ nanocrystals over a broad range of compositions, $0.30 < x < 0.87$. Control of x was achieved by nitridation of nanocrystalline $ZnGa_2O_4$ and ZnO precursors in varying ratios. Use of nanoscale precursors and relatively low nitridation temperatures prevented both the formation of bulk oxy(nitride) and the evaporation of Zn, and this strategy produced high-quality nanocrystals. Over the range of compositions studied, the absorption onset decreased monotonically from 2.7 to 2.2 eV with increasing x, which corresponds to a 260% improvement in solar photon absorption. We expect that the nanocrystalline morphology as well as the tunable composition and band gap will prove beneficial for the use of $(Ga_{1-x}Zn_x)(N_{1-x}O_x)$ in solar photochemistry.

■ ASSOCIATED CONTENT

Supporting Information

Synthesis and characterization methods; TEM images and XRD patterns of starting materials; elemental analysis for starting materials and products of 650 °C nitridation; TEM images and size analysis of $(Ga_{1-x}Zn_x)(N_{1-x}O_x)$ nanoparticles with x = 0.54, 0.66, 0.76, and 0.87; and photograph of samples with varying values of x. This material is available free of charge via the Internet at http://pubs.acs.org.

■ AUTHOR INFORMATION

Corresponding Author

*E-mail: Gordana.Dukovic@colorado.edu

Notes

The authors declare no competing financial interest.

■ ACKNOWLEDGMENTS

This work was supported by the University of Colorado Boulder startup funds and seed funding from Center for Revolutionary Solar Photoconversion. B.M.T. was supported by a fellowship from ConocoPhillips. Special thanks to S. George for loan of the high-temperature furnace, and A. Prieto, C. Rithner, S. Fredrick, and L. Wally for access to the Chemical Instrumentation Facility at Colorado State University. We also thank J. Eaves for helpful discussions. Diffuse reflectance spectra were taken at the National Renewable Energy Laboratory, and aberration-corrected HRTEM images were obtained at the CAMCOR facility at the University of Oregon. The CAMCOR High-Resolution and Nanofabrication Facilities are supported by grants from the W. M. Keck Foundation, the M.J. Murdock Charitable Trust, ONAMI, the Air Force Research Laboratory (agreement no. FA8650-05-1-5041), NSF (award nos. 0923577 and 0421086), and the University of Oregon.

REFERENCES

(1) Maeda, K.; Domen, K. *J. Phys. Chem. C* **2007**, *111* (22), 7851−7861.
(2) Maeda, K.; Domen, K. *Chem. Mater.* **2010**, *22* (3), 612−623.
(3) Maeda, K.; Domen, K. *J. Phys. Chem. Lett.* **2010**, *1* (18), 2655−2661.
(4) Maeda, K.; Teramura, K.; Lu, D. L.; Takata, T.; Saito, N.; Inoue, Y.; Domen, K. *Nature* **2006**, *440* (7082), 295−295.
(5) Chen, H. Y.; Wang, L. P.; Bai, J. M.; Hanson, J. C.; Warren, J. B.; Muckerman, J. T.; Fujita, E.; Rodriguez, J. A. *J. Phys. Chem. C* **2010**, *114* (4), 1809−1814.
(6) Di Valentin, C. *J. Phys. Chem. C* **2010**, *114* (15), 7054−7062.
(7) Dou, M.; Persson, C. *Phys. Status Solidi A* **2012**, *209* (1), 75−78.
(8) Hirai, T.; Maeda, K.; Yoshida, M.; Kubota, J.; Ikeda, S.; Matsumura, M.; Domen, K. *J. Phys. Chem. C* **2007**, *111* (51), 18853−18855.
(9) Huda, M. N.; Yan, Y. F.; Wei, S. H.; Al-Jassim, M. M. *Phys. Rev. B* **2008**, *78* (19), 195204/1−5.
(10) Jensen, L. L.; Muckerman, J. T.; Newton, M. D. *J. Phys. Chem. C* **2008**, *112* (9), 3439−3446.
(11) Lee, Y. C.; Lin, T. Y.; Wu, C. W.; Teng, H. S.; Hu, C. C.; Hu, S. Y.; Yang, M. D. *J. Appl. Phys.* **2011**, *109* (7), 073506/1−5.
(12) Li, L.; Muckerman, J. T.; Hybertsen, M. S.; Allen, P. B. *Phys. Rev. B* **2011**, *83* (13), 134202/1−6.
(13) McDermott, E. J.; Kurmaev, E. Z.; Boyko, T. D.; Finkelstein, L. D.; Green, R. J.; Maeda, K.; Domen, K.; Moewes, A. *J. Phys. Chem. C* **2012**, *116* (14), 7694−7700.
(14) Wang, S. Z.; Wang, L. W. *Phys. Rev. Lett.* **2010**, *104* (6), 065501/1−4.
(15) Wei, W.; Dai, Y.; Yang, K.; Guo, M.; Huang, B. *J. Phys. Chem. C* **2008**, *112* (40), 15915−15919.
(16) Yoshida, M.; Hirai, T.; Maeda, K.; Saito, N.; Kubota, J.; Kobayashi, H.; Inoue, Y.; Domen, K. *J. Phys. Chem. C* **2010**, *114* (36), 15510−15515.
(17) Yu, H. G. *Chem. Phys. Lett.* **2011**, *512* (4−6), 231−236.
(18) Wang, J. P.; Huang, B. B.; Wang, Z. Y.; Wang, P.; Cheng, H. F.; Zheng, Z. K.; Qin, X. Y.; Zhang, X. Y.; Dai, Y.; Whangbo, M. H. *J. Mater. Chem.* **2011**, *21* (12), 4562−4567.
(19) Hisatomi, T.; Maeda, K.; Takanabe, K.; Kubota, J.; Domen, K. *J. Phys. Chem. C* **2009**, *113* (51), 21458−21466.
(20) Maeda, K.; Teramura, K.; Domen, K. *J. Catal.* **2008**, *254* (2), 198−204.
(21) Kay, A.; Cesar, I.; Gratzel, M. *J. Am. Chem. Soc.* **2006**, *128* (49), 15714−15721.
(22) Sabio, E. M.; Chamousis, R. L.; Browning, N. D.; Osterloh, F. E. *J. Phys. Chem. C* **2012**, *116* (4), 3161−3170.
(23) Han, W. Q.; Liu, Z. X.; Yu, H. G. *Appl. Phys. Lett.* **2010**, *96* (18), 183112/1−3.
(24) Han, W. Q.; Ward, M. J.; Sham, T. *J. Phys. Chem. C* **2011**, *115* (10), 3962−3967.
(25) Han, W. Q.; Zhang, Y.; Nam, C. Y.; Black, C. T.; Mendez, E. E. *Appl. Phys. Lett.* **2010**, *97* (8), 083108/1−3.
(26) Byun, H. J.; Kim, J. U.; Yang, H. *Nanotechnology* **2009**, *20* (49), 495602/1−6.
(27) Becheri, A.; Durr, M.; Lo Nostro, P.; Baglioni, P. *J. Nanopart. Res.* **2008**, *10* (4), 679−689.
(28) Amirav, L.; Alivisatos, A. P. *J. Phys. Chem. Lett.* **2010**, *1* (7), 1051−1054.
(29) Maeda, K.; Teramura, K.; Takata, T.; Hara, M.; Saito, N.; Toda, K.; Inoue, Y.; Kobayashi, H.; Domen, K. *J. Phys. Chem. B* **2005**, *109* (43), 20504−20510.
(30) Joo, J.; Kwon, S. G.; Yu, J. H.; Hyeon, T. *Adv. Mater.* **2005**, *17* (15), 1873−1877.
(31) Sun, X.; Maeda, K.; Le Faucheur, M.; Teramura, K.; Domen, K. *Appl. Catal., A* **2007**, *327* (1), 114−121.
(32) Yashima, M.; Yamada, H.; Maeda, K.; Domen, K. *Chem. Commun.* **2010**, *46* (14), 2379−2381.
(33) Chen, H.; Wen, W.; Wang, Q.; Hanson, J. C.; Muckerman, J. T.; Fujita, E.; Frenkel, A. I.; Rodriguez, J. A. *J. Phys. Chem. C* **2009**, *113* (9), 3650−3659.
(34) Tolbert, S. H.; Alivisatos, A. P. *Annu. Rev. Phys. Chem.* **1995**, *46* (1), 595−626.
(35) Suryanarayana, C.; Grant Norton, M. *X-Ray diffraction: a practical approach*; Plenum Press: New York, 1998.
(36) Tauc plots for a direct-gap semiconductor give band gaps that are red-shifted by ∼0.1 eV, while those for an indirect-gap material are blue-shifted by ∼0.1 eV.
(37) Calculations were carried out using the AM 1.5 terrestrial solar spectrum (ASTM G173).
(38) Gerischer, H. *J. Electrochem. Soc.* **1966**, *113* (11), 1174−1182.
(39) Maeda, K.; Takata, T.; Hara, M.; Saito, N.; Inoue, Y.; Kobayashi, H.; Domen, K. *J. Am. Chem. Soc.* **2005**, *127* (23), 8286−8287.